On the Difference in Mechanical Behavior of Glass Bead-Filled Polyamide 12 Specimens Produced by Laser Sintering and Injection Molding

De Coninck Hellen[1]*, Meyers Sebastian[1], Van Puyvelde Peter[2], Van Hooreweder Brecht[1]

[1]KU Leuven, Department of Mechanical Engineering, Manufacturing Processes and Systems (MaPS) , Celestijnenlaan 300, 3001 Leuven, Belgium
[2]KU Leuven, Department of Chemical Engineering, Soft Matter, Rheology and Technology (SMaRT), Celestijnenlaan 200J, 3001 Leuven, Belgium

This is the accepted version of the following article: On the Difference in Mechanical Behavior of Glass Bead-Filled Polyamide 12 Specimens Produced by Laser Sintering and Injection Molding, which has now been formally published in final form at 3D Printing and Additive Manufacturing at https://doi.org/10.1089/3dp.2022.0160. This original submission version of the article may be used for non-commercial purposes in accordance with the Mary Ann Liebert, Inc., publishers' self-archiving terms and conditions.

Authorship contribution statement:
Hellen De Coninck: Methodology, Formal analysis, Investigation, Writing–Original Draft, Visualization
Sebastian Meyers: Methodology, Formal analysis, Writing-Review and Editing
Peter Van Puyvelde: Writing-Review and Editing
Brecht Van Hooreweder: Methodology, Formal analysis, Writing-Review and Editing, Supervision

Abstract

An increasing demand for additively manufactured polymer composites with optimised mechanical properties is manifesting in different industries such as aerospace, biomedical and automotive. Laser sintering (LS) is an additive manufacturing (AM) method that has the potential to produce reinforced polymers which can meet the stringent requirements of these industries. For the development of a commercially viable LS nylon-based composite material, previous research studies worldwide have focused on adding glass beads to the powder material with the goal to produce fully dense parts with properties more representative of injection moulded thermoplastic composites. This led to the development of a commercially available glass bead filled polyamide 12 (PA12) powder. Although this powder has been on the market for quite a while, an in-depth comparison of the mechanical behaviour of laser sintered versus injection moulded glass bead filled PA12 is lacking. In this study, laser sintered glass bead filled PA12 samples were built in different orientations and compared to injection moulded counterparts. After sample production, the mechanical performance of the produced LS and IM parts was tested and compared to evaluate the quasi-static and dynamic mechanical performance and failure mechanisms at different load levels. In addition, the glass bead filled PA12 properties were also compared to those of standard (unfilled) LS PA12 in order to assess whether glass beads actually improve the mechanical performance and fatigue lifetime of the final LS samples, as suggested in literature. Results in this work present and explain the increased stiffness but decreased fatigue life of glass bead filled polyamide parts made by LS and IM. This research can be regarded as a 'benchmark' study in which samples produced from commercially available, filled and unfilled, PA12 powder grades are compared for both laser sintering and conventional production techniques.

Keywords: Laser sintering / Injection moulding / Polyamide 12 / Filled polymers / Fatigue performance

*Principal corresponding author *(hellen.deconinck@kuleuven.be)*

1 Introduction

Laser sintering (LS) is a powder based additive manufacturing (AM) process for polymers, metals and ceramics [1, 2]. Layers of preheated powder are spread on a build platform and subsequently scanned by a laser beam that consolidates powder together to form a cross section of the desired component. The sintered material forms the component, whilst the unsintered material remains in place to support it [3, 4]. Polymer powders were the first and are still the most widely applied materials in LS. The most used polymers are semi-crystalline thermoplastics, like polyamide 12 (PA12) [1, 2]. LS is considered the best AM technique for structural polymer parts as the final part density approaches full density, and their properties may reach those of similar bulk material, leading to durable and strong AM components [5]. As LS was evolving from a rapid prototyping technique towards rapid manufacturing, a need surfaced for a broader material palette with improved mechanical performance, such as high structural strength and stiffness [4, 6]. A way of increasing part strength is by using reinforcements to produce reinforced composite materials. This suits the LS process, since it already processes the polymers that are typically used as matrix materials [2, 4]. Attempts to improve mechanical and physical properties by reinforcing raw polymer powder with nanoscale and microscale fibres have been carried out and led to the development of various composite polymer powders as reported in [7–14].

For the development of a commercially viable LS polyamide based composite material, several studies researched glass beads as reinforcement with the goal to produce fully dense parts with properties more representative of injection moulded (IM) thermoplastic composites. For injection moulded composites, the matrix material typically consists of a ductile thermoplastic reinforced with short fibres or a particulate. The LS composite research was targeted at homogeneously mixing the composite powder, as isotropic systems offer many of the advantages of a fibre reinforced material without the complications of anisotropic shrinkage and anisotropic mechanical properties [15, 16]. Amongst others, Forderhase et al. have performed a comparison on the quasi-static and material properties of filled and unfilled LS samples and concluded that the resulting laser sintered polymer parts filled with glass beads typically have a much higher modulus of elasticity compared to unfilled counterparts, though only a small improvement in strength can typically be noticed [16]. Cano et al. investigated the influence of orientation and temperature on the mechanical properties of glass bead filled and unfilled polyamide powder and concluded that the fracture resistance of unfilled, regular PA12 was higher compared to the filled material due to the poor adhesion of the glass beads to the matrix [17]. However, an extension towards fatigue behaviour and a comparison with injection moulded counterparts produced from the same material is currently still missing in scientific literature. An extensive investigation of the fatigue life of laser sintered polyamide 12 was done by Salazar et al. from which can be concluded that crazing is the main mechanism responsible of nucleation and growth of damage until a macroscopic crack is generated and further crack advancement occurs [18]. Though, no comparison with another material produced by LS or other production technique was included. Compared to conventional production techniques, such as IM, the LS process has many potential advantages: short cycle times from design to manufacturing, customized components, high geometrical freedom and inexpensive production of small batches of parts. However, to be able to compete with conventional production techniques, the mechanical properties of LS components should be optimised to meet operational requirements and in service loading [3].

In previous research, a comparison of the material structure and fatigue properties of unfilled polyamide samples produced by IM and LS was carried out [3]. In the present work, similar detailed research was performed for glass bead filled PA12 LS and IM samples. All the samples were produced from the same powder and both mechanical and fatigue testing were conducted after careful examination of the quality of the end-products. Consequently, for the first time, a true comparison between IM and LS glass bead filled PA12 samples was made. In addition, steps from the previous research conducted by Van Hooreweder et al. were repeated [3]. Regular, unfilled PA12 samples were laser sintered with similar parameters and in similar conditions as the LS production of the glass bead filled PA12 samples. To compare these LS samples with samples produced with a conventional production technique, compression moulded (CM) PA12 samples were investigated. Again, both mechanical and fatigue testing were conducted on the regular, unfilled PA12 samples after examination of the quality of the end-products.

The broader goal of this research is to investigate the commercially available glass bead filled polyamide powder and find out the properties of parts produced with this powder by laser sintering and conventional manufacturing techniques, in this case injection moulding. This leads to concrete insights that can help understanding if the glass bead filled polyamide powder can meet the increasing demand for additively manufactured polymer composites with optimised mechanical properties, such as high structural strength and stiffness, considering the stringent requirements of industries such as

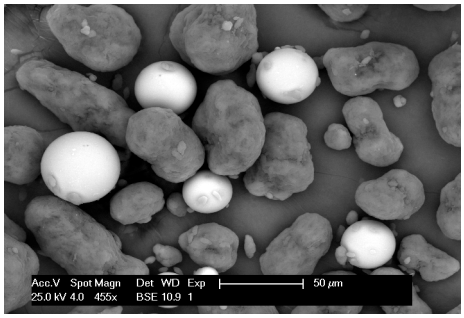

Figure 1: SEM image of glass bead filled PA12 (PA 3200 GF) powder particles and glass beads

Table 1: Process parameters for extrusion of glass bead filled PA12 powder

parameter	unit	
Heating zone 1 (Hopper)	[°C]	163
Heating zone 2	[°C]	185
Heating zone 3	[°C]	199
Heating zone 4	[°C]	199
Heating zone 5	[°C]	199
Heating zone 6 (Die)	[°C]	190
Screw rotation speed	[rpm]	18-20

aerospace, biomedical and automotive.

2 Test samples

2.1 Material

Glass bead filled polyamide 12 powder (PA 3200 GF, EOS, d50 = 57µm) was used as base material for sample production with LS and IM in this work. After CT scanning, a volume percentage of 15,5% of glass beads in the PA12 powder was defined. Regular, unfilled polyamide 12 powder (PA 2200, EOS, d50 = 56µm) was used as base material for sample production with LS. Powder dimensions and properties have an important influence on the final quality of parts produced by LS. Only two batches of the glass filled, semi-crystalline polyamide 12 powder material (PA 3200 GF) were used to minimise the influence of the raw material on the mechanical properties of the produced specimens for both LS and IM. The regular, unfilled LS samples were built with one batch of powder. In both cases, a mix of 25% recycled and 75% virgin powder was used [19]. A scanning microscope (SEM, FEI XL30-FEG) observation of the glass filled PA12 powder, indicating particles with an average diameter of 57µm and a semi-spherical geometry, is shown in Figure 1. Although different processing steps for both the LS and IM processes lead to different thermal histories, molecular structures and properties which will influence the final part quality, the same polyamide powder was used where possible to have a 'starting point' for further comparison of the samples.

2.2 Pellet preparation

The same glass bead filled polyamide powder (PA 3200 GF, EOS) used for the LS process, was also used to produce pellets used as starting material for the injection moulding process. In this case, 100% virgin powder was used as opposed to the mix of 25% recycled and 75% virgin powder in the LS process. The pellets were produced using a Collin extruder with a cylinder nominal diameter of 25 mm. The heating system of the single screw extruder is divided in six heating zones which can be regulated separately. The process parameters are listed in Table 1. The extruder is accompanied by a water bath to cool the extruded filament and by a pelletizer to cut the filament into pellets. The pellet length was set at 2,8 mm.

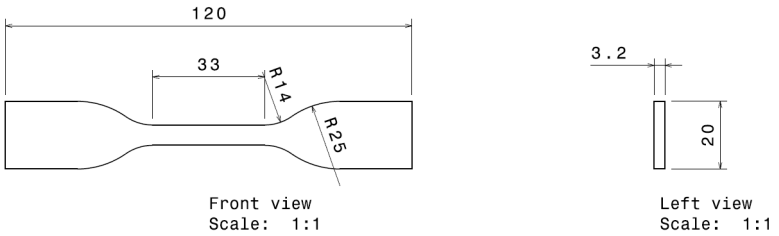

Figure 2: Geometry of specimens produced by LS and CM (ASTM-D638 Type IV Tensile Test Specimen) (all dimensions in mm)

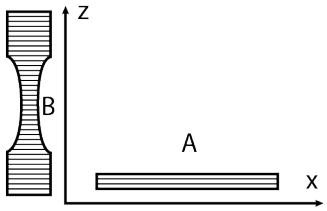

Figure 3: Scan direction for the LS samples, LSx (A) and LSz (B) [3]

2.3 Sample design

The geometry of the specimens produced by IM is according to ISO 527-2 (dumbbell-shaped with a gauge length of 50 mm and thickness of 4 mm). With this geometry the parts could be subjected to tension-tension stresses in a uni-axial fatigue testing machine (Instron ElectroPuls). Figure 2 shows the geometry of the specimens produced by LS and CM, according to ASTM D638 type IV. This standard was preferred as it specifies smaller samples, limiting production time and powder consumption. During the laser sintering process, the test samples were built in two directions, including the z-direction (perpendicular to the powder bed) and the X-direction (parallel to the powder bed). Again, the produced specimens by LS and CM are suitable to be subjected to tension-tension stresses during uni-axial fatigue testing. Previous work by the authors has shown no statistically significant difference in polymer tensile or fatigue properties for the ISO 527-2 sample geometry compared to the ASTM D638 type IV sample geometry [20].

2.4 Laser sintering

The test samples were produced by laser sintering from the above discussed glass bead filled PA12 powder (PA3200 GF, EOS) and regular, unfilled PA12 powder (PA2200, EOS). To study the influence of the build and scanning direction on the mechanical properties, the samples were built in two different directions. With the glass bead filled PA12 powder 30 samples were built in the x-direction (longitudinal axis) and 35 samples in the z-direction, all in the same build job. With the regular, unfilled PA12 powder 12 samples were built in the x-direction and 20 in the z-direction.

Table 2 shows the LS process parameters used for this study. To find these, a profound parameter optimisation based on Archimedes density measurements was done. Various batches of cubes and bars were scanned in order to find the optimal processing window. Laser powers (P) from 12 to 38 W and scanning speeds (v) from 150 to 1500 mm/s were used. The layer thickness (l) was kept constant at 100 µm and scan spacing (s) at 150 µm. The optimised process parameters from Table 2 resulted in final parts with relative densities above 98% when compared to IM and CM samples.

To minimise scatter in the mechanical properties, all the samples were manufactured using the same LS machine, a commercial DTM Sinterstation 2000 equipped with a CO2-laser. Though, due to technical problems (severe degradation of the CO2-laser resulting in reduced laser power in the build chamber), the laser was replaced in between build jobs. The glass bead filled PA12 samples were built with the initial laser with degradation, the regular, unfilled PA12 samples were built with a new CO2-laser. To give an estimation of the 'real' energy densities used during production of the glass filled samples, the actual laser power was measured with an Ophir Nova power and energy meter (P/N 7Z01500) in the build chamber and estimated values for the used energy densities are shown in Table 2. During LS processing, an inert

Table 2: Process parameters for laser sintering of glass bead filled PA12 powder (PA 3200 GF, EOS) and regular, unfilled PA12 powder (PA 2200, EOS)

material		PA 3200 GF	PA 2200
parameter	unit		
Average grain size	[µm]	57	56
Sintering temp.	[°C]	170	170
Removal chamber temp.	[°C]	30	30
Scan spacing	[mm]	0.15	0.15
Feed temp.	[°C]	60	60
Layer thickness	[µm]	100	100
Energy density (x)	[J/mm^3]	0.72	0.53
Energy density (z)	[J/mm^3]	0.64	0.50

Table 3: Process parameters for injection moulding of glass bead filled PA12 pellets

parameter	unit	
Mould temp.	[°C]	85
Nose temp.	[°C]	300
Hopper temp.	[°C]	80
Injection pressure	[bar]	1000
Injection speed	[mm/s]	70
Hold pressure	[bar]	600
Hold time	[s]	8
Cooling time	[s]	25

nitrogen atmosphere was used and a powder bed preheating temperature of 170°C for both materials. No post-processing was applied after laser sintering thus the as-built material behaviour was studied.

2.5 Injection moulding

Pellets are needed as starting material for the injection moulding process. These were made, as mentioned in 2.3, by extruding the powder material and pelletizing the produced filament. The same starting material was used in order to accurately compare the influence of the different production techniques (LS and IM) on the mechanical properties of the produced samples. The pellets were dried for 4 hours at 80 °C prior to injection moulding using a hot air oven (Piovan). This to limit moisture in the starting material that could have a deteriorating effect on the mechanical properties of the final samples.

Table 3 shows the process parameters for a Demag Intellect 50 injection moulding machine which was used to produce the samples. After the injection moulding process, no post-treatment was applied and so the as-moulded material behaviour was studied. Care has been taken to choose process parameters that do not induce too much orientation effects within the parts. The molar masses of PA12 are low and hence, relaxation times are small (typically ¡ 1s). After IM, eventual orientation will have relaxed during the relatively slow cooling process. Hence, no significant effect of residual orientation on the mechanical properties is expected.

2.6 Reference compression moulded samples

For the regular, unfilled CM samples a commercial compression moulded PA12 plate (VINK) was ordered with dimensions 2000x1000x3mm. From this plate 100 samples were cut with a waterjet in the geometry shown in Figure 2. Waterjet cutting was used to avoid heating of the CM PA12 material. After the waterjet cutting the samples were dried and no further post-processing was applied so the compression moulded material behaviour was studied.

3 Experimental analysis

3.1 Material and sample characterisation

For the glass bead filled PA12 samples produced by LS and IM, the same raw material was used for the production processes. Nevertheless, the material structure was not the same, leading to different mechanical properties and different failure mechanisms. For the regular PA12 different raw materials were used for the LS and CM processes. To be able to properly analyse the results and to get a better understanding of the differences in mechanical properties and fatigue performance of the LS, IM an CM samples, the sample/material quality after different production steps was studied as described below.

3.1.1 CT scanning

CT scanning was performed on a representative powder batch of the glass bead filled PA12 using a 180 kV Nanotom s CT system (GE, Baker Hughes), with a molybdenum target, a voltage of 70 kV, a current of 220 µA and 2400 projections. A 0,2 mm thick aluminium filter was installed to remove low energy photons from the X-ray spectrum. The magnification of 33,34 allowed to obtain a voxel size of 1,5 µm. Voxel reconstruction was performed in DatosX software. Segmentation of the dataset and quantitative analysis was performed in Avizo 2021.2, where a grey-scale thresholding was used to differentiate between glass beads and polymer matrix.

3.1.2 Dimensions of the critical cross sections

The critical cross-section is most important in dog bone tensile samples as it determines the region where failure will occur. The cross-sections were measured by a set of Vernier callipers (Mitutoyo). Width and thickness of the samples were measured and taken into account when calculating the stress in the cross-sections during the tensile tests and fatigue tests. For each material and production process, six samples were measured and from the thickness and width, the cross-sections were calculated.

3.1.3 Microscopy

Observation of the morphology of the powder material and observations of the fracture surfaces after fatigue testing were done using scanning electron microscopy (SEM, FEI XL30-FEG). Fracture profiles of the samples after fatigue testing were assessed using a digital 3D microscope Keyence VHX-6000.

3.1.4 Microstructure

Differential Scanning Calorimetry (DSC) tests were carried out after every production step to compare the thermal influence on the resulting material and the degree of crystallinity of the produced samples. These tests were performed on a Q2000 DSC (TA Instruments) machine. For these tests, 9,25 ± 0,25 mg of material was collected from the powder, from the pellets before and after drying, and from the produced IM, CM and LS samples. These material samples were each time subjected to a temperature scan from 20 °C to 240 °C and back with a heating and cooling rate of 10 °C/min. Properties of polymer samples are significantly influenced by their degree of crystallinity. The higher the degree of crystallinity, the stiffer and stronger, but also more brittle the polymers parts tend to be [21].

The heat of melting in J/g is represented by the area of the melting peaks. Equation 1 expresses the percentage of crystallinity (C%) of the semi-crystalline material PA12 [3]. As it is only the polymer material that will be sintered only these melting peaks will be taken into account.

$$C_{\%} = \frac{\textit{Heat of melting (sample)}}{\textit{Heat of melting (100\% crystalline specimen)}} \tag{1}$$

In order to calculate the crystallinity of the glass filled samples, the equation has to be modified. Since a fraction of the material is glass, which has a much lower specific heat than PA12, an estimation of the real crystallinity of the sample can be obtained by using the following equation 2:

$$X_{\mathrm{C}} = \frac{\Delta H_C}{\Delta H_f \cdot (1 - m_g)} \cdot 100\% \tag{2}$$

Where m_g is the mass fraction of glass in the composite [22].

Figure 4: Roughness measurement scan track over the narrow section of the sample

3.1.5 Density

Densities of laser sintered, compression moulded and injection moulded parts were assessed by the Archimedes method (Acculab atilon ATL-244-1). These density measurements were done during the optimisation process to find the optimal LS parameters (see Table 2) that were selected to produce dense parts. The densities of the LS parts were compared to the density of bulk PA12 and to the density of IM parts.

3.1.6 Hardness

Shore D hardness tests were performed using a manual Zwick 3116/7 apparatus. Three-point measurements were done on each sample. From each material and production process, three samples were measured.

3.1.7 Surface roughness

Surface roughness measurements were done on a Mitutoyo Formtracer CS-3200 machine with a 60deg conical probe and 2 µm tip radius. Three straight scan tracks with a sample length of 48mm were measured over the narrow section of the samples as can be seen in Figure 4, at a speed of 0,20 mm/sec. This way 2D topography profiles were recorded and with the software related to the machine the Ra, Rz and Rk-values were obtained. For each material and production process, three samples were measured.

3.2 Mechanical characterisation

Tensile tests were conducted on an Instron 3367 quasi-static machine with a 5 kN load cell and an Instron AVE2 video-extensometer. The tests were conducted at 5 mm/min. The results of these tensile tests were used to determine the first stress amplitude for the fatigue testing which was fixed at 60% of the UTS. A minimum of 6 samples were tested from each production process (LS (x and z), IM and CM) and for each material (PA3200 GF, PA2200 and PA12). For each sample the width and thickness of the test section of the samples was measured and used as input for the Instron software to calculate the dimensions of the cross-sections of the samples and subsequently the correct stress values.

Fatigue tests were performed on an Instron Electropuls E10000 machine with a 10 kN load cell, a sinusoidal loading frequency of 3 Hz and load ratio R = 0.1. Two devices were used for the temperature measurements: a pyrometer and a thermocouple. The pyrometer was used for contact-free measurement of the thinnest cross-section of the test samples whilst the thermocouple was used to measure the environment temperature which was kept constant between 20-22°C. By subtracting the room temperature from the sample surface temperature measurements, the actual heat dissipation during testing was measured and was not influenced by environment influences such as room heating or cooling. At least 10 samples were tested from each production process and for each material. No artificial cooling was applied. Careful attention was given to a proper alignment of the test specimens in order to avoid secondary bending stresses.

4 Results and discussion

4.1 Sample characteristics

The heat of melting for a 100% crystalline PA12 specimen produced by PA12 equals 209,3 J/g according to Gogolewski et al. [3, 23], which was used to calculate the crystallinity of the regular, unfilled PA12 samples with Equation 1. Equation 2 yields a percentage of crystallinity of 24% for the LSx samples, 18% for the LSz samples and 21% for the IM samples produced with the glass bead filled PA12 powder. The DSC curves of the different samples can be seen in Figure 5.

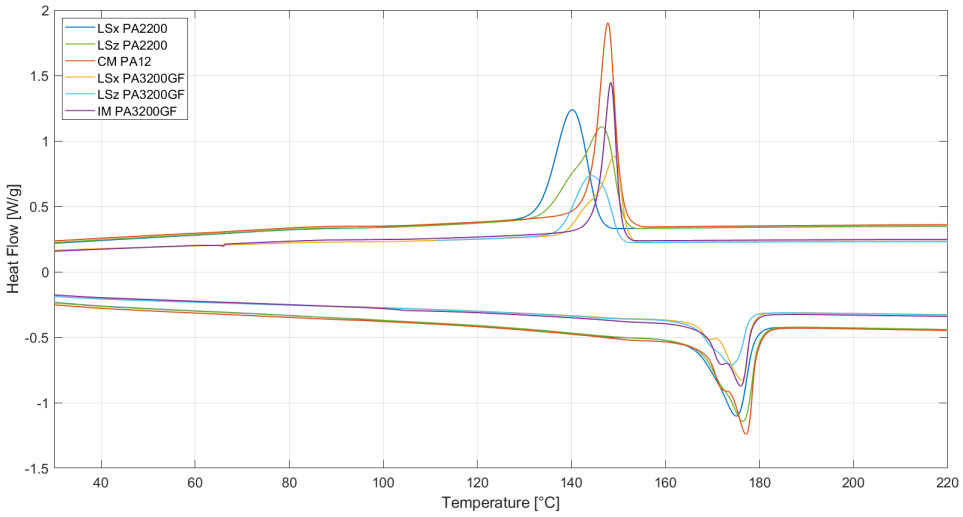

Figure 5: DSC curves from the produced samples (different materials glass bead filled PA12 and regular, unfilled PA12 (PA3200 and PA2200, PA12, respectively) and manufacturing processes (LSx, LSz, CM, IM)). Each DSC curve represents 1 sample tested

The cross-sections, densities, Shore D hardness values, Ra, Rz and Rk roughness values, melting temperatures and calculated crystallinity values are summarized in Table 4 for all the produced samples. The average width and thickness of the samples to calculate the cross-sections for mechanical testing are summarized in Table 5.

4.2 Comparison glass bead filled PA12 produced by LS and IM

In this section, only the glass bead filled PA12 (PA3200 GF) samples are taken into consideration. The focus is laid on the comparison of production techniques (LS and IM) and build orientations (LSx and LSz).

4.2.1 Quasi-static performance

To determine appropriate stress levels to be applied during fatigue testing, tensile tests were performed on samples of each category (production processes: LS, IM and CM and materials: glass bead filled PA12 (PA3200 GF), regular, unfilled PA12 (PA2200 and PA12)). The results of these tests are summarized in Table 6 and the tensile curves of these tests are shown in Figure 6.

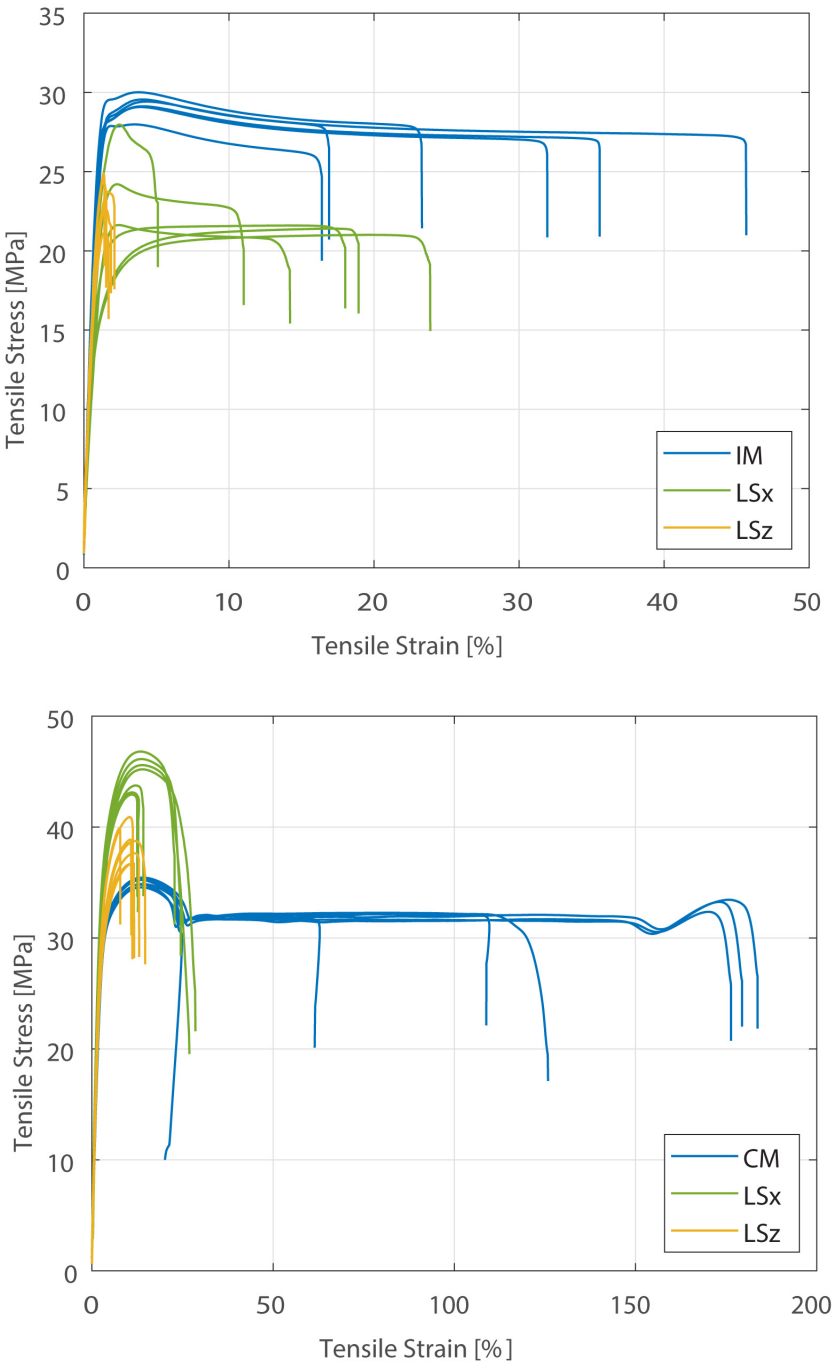

Figure 6: Tensile curves of the tensile tests performed on the glass bead filled (PA3200 GF) samples (top) and regular, unfilled PA12 (PA2200 and PA12) (bottom)

Table 4: Properties of produced samples

material		glass bead filled PA12 (PA3200 GF)		
parameter	unit	LSx	LSz	IM
cross-section	[mm^2]	27,91±0,725	29,22±0,534	41,25±0,472
density	[%]	99,57	98,69	ref.
hardness	Shore D	75±0,8	74±1,2	74±1,0
Ra-value	[µm]	19,18±0,389	24,66±2,872	0,26±0,026
Rz-value	[µm]	131,59±1,365	164,18±18,309	2,48±0,163
Rk-value	[µm]	63,08±1,799	80,82±9,909	0,71±0,023
melting T	[°C]	179	176	179
crystallinity	[%]	24	18	21

material		regular PA12 (PA2200)		regular PA12
parameter	unit	LSx	LSz	CM
cross-section	[mm^2]	18,95±0,384	23,54±1,342	19,78±0,072
density	[%]	99,79	98,63	ref.
hardness	Shore D	72±2,3	73±1,8	74±1,9
Ra-value	[µm]	17,41±1,331	20,31±1,032	0,32±0,195
Rz-value	[µm]	124,09±13,022	138,90±12,500	1,84±0,553
Rk-value	[µm]	55,68±3,952	65,42±3,132	0,25±0,058
melting T	[°C]	181	180	179
crystallinity	[%]	28	32	15

Table 5: Dimensions for calculations of the cross-sections of produced samples used for tensile testing

material		glass bead filled PA12 (PA3200 GF)		
parameter	unit	LSx	LSz	IM
Width	[mm]	6,91±0,07	6,93±0,05	10,23±0,11
Thickness	[mm]	4,01±0,06	4,22±0,05	4,06±0,05

material		regular PA12 (PA2200)		regular PA12
parameter	unit	LSx	LSz	CM
Width	[mm]	5,87±0,05	6,42±0,16	6,13±0,03
Thickness	[mm]	3,22±0,06	3,60±0,15	3,23±0,02

The following phenomena are noted.

- Only a small difference in ultimate tensile strength (UTS) is noted between LS and IM samples. IM samples are slightly stronger, with a UTS value of 29 MPa compared to 24 and 23 MPa for LSx and LSz samples respectively.
- The difference in modulus of elasticity and fracture strain indicate that the LS samples are more brittle than the IM samples. It is expected that because of the applied temperature and pressuring during IM, samples with a higher density are produced with good adhesion of the glass beads to the polyamide matrix which leads to the higher values of strength and stiffness.
- LSx and LSz samples indicate similar values for UTS and modulus of elasticity (E-modulus). However, the ϵ-fracture is much lower in the LSz samples which indicates that for quasi static loading, intralayer fracture (within layers) is less brittle then interlayer fracture (between successive layers) [3].

These results are consistent with previous research comparing the difference in material structure and fatigue properties of regular, unfilled PA12 specimens produced by IM and LS [3].

4.2.2 Fatigue performance

The results of the fatigue experiments are presented in Figure 7 as six SN curves on a double logarithmic scale. Also the ultimate tensile strength values from Table 6 are included in Figure 7 as can be seen on

Table 6: Results of tensile tests

material		glass bead filled PA12 (PA3200 GF)		
parameter	unit	LSx	LSz	IM
UTS	[MPa]	24±2,6	23±1,4	29±0,7
E-modulus	[MPa]	1518±487,1	1958±165,0	2440±164,5
ϵ-fracture	[%]	13±8,3	2±0,3	28±11,5

material		regular PA12 (PA2200)		regular PA12
parameter	unit	LSx	LSz	CM
UTS	[MPa]	45±1,5	38±1,6	35±0,3
E-modulus	[MPa]	1367±101,4	1161±71,4	1061±20,1
ϵ-fracture	[%]	20±6,9	12±2,1	123±62,1

the vertical axis at load cycle 1. It is important to notice that these quasi-static stress values (UTS) are determined at very low strain rate (5mm/min) compared to the stress values plotted for the fatigue tests carried out at 3Hz **(˜100mm/min)**. For that reason, the UTS values are not included for the curve fitting in Figure 7. Thus, except for the UTS values (datapoints at 10^0), all datapoints are included for the curve fitting. When plotted on a double logarithmic scale, the datapoints closely match a straight line following the Basquin law with equation 3:

$$S_f = A \cdot (N_f)^B \tag{3}$$

Where S_f is the fatigue strength and N_f the cycles to failure. A and B are constant used to plot the lines and are given in the legend of Figure 7 together with the R^2 constants.

Figure 8 shows the temperature accumulation of the outer surface of samples produced by LS (in the x- and z-direction) and produced by IM during fatigue testing on a semi-logarithmic scale. This accumulation was obtained by comparing the ambient temperature and the temperature of the sample (measured by a thermocouple and a pyrometer, respectively) as a function of the number of load cycles to failure.

The variation between the SN-curves of the LSx and IM samples is limited which means that samples show similar fatigue behaviour under the same test conditions. For the LSz samples, the SN-curve is lowest and has a steeper slope compared to the SN-curves of the LSx and IM samples. Samples build along the build direction (z-direction) are known to have a lower ductility and strength as they are sensitive to varying process conditions and imperfect bonding between consecutive layers due to the interlayer building time which is larger than the intralayer building time. The stacking-layer-process happening during the building of the samples can lead to insufficient interlayer connection resulting in pore formation and residual particles. These pores and particles can occur with varying frequency and morphology (size, shape, orientation) [24]. It is well-known that pores and residual particles have a significant influence on fatigue behaviour of polymers as they can act as crack initiators [25]. As noted in the results of the tensile tests, the assumption was also made that intralayer fracture (within layers) is less brittle than interlayer fracture (between successive layers). This is confirmed by microscopy images of the fracture profiles of a LSx and LSz sample after fatigue testing, which can be seen in Figure 9 and can explain the lower and steeper slope of the SN-curve of the LSz samples. This was also concluded by Salazar et al. after fatigue testing of regular, unfilled PA12 under similar conditions [18].

In general, the fatigue tests resulted in brittle fracture surfaces which is assumed to be a result from the presence of the glass beads which will be further discussed in section 4.3. Scanning microscopy observations of the fracture surfaces of the glass bead filled PA12 samples can be seen in Figure 10.

4.2.3 Hysteresis

As noted by Van Hooreweder et al. [3], fatigue failure of polymers is typically caused by a combination of mechanical and thermal loading. Also during this study, no artificial cooling and a fixed test frequency of 3 Hz was applied which makes that the temperature increase in the material (self-heating) plays an important role in the fatigue life of the samples. A pyrometer was used during fatigue testing for contact-free temperature measurement of the cross-section of the test samples. Figure 8 shows the temperature accumulation of glass bead filled PA12 samples produced by LS and IM during fatigue testing. Towards the final cycles to failure, an increase in temperature can be noted until final failure.

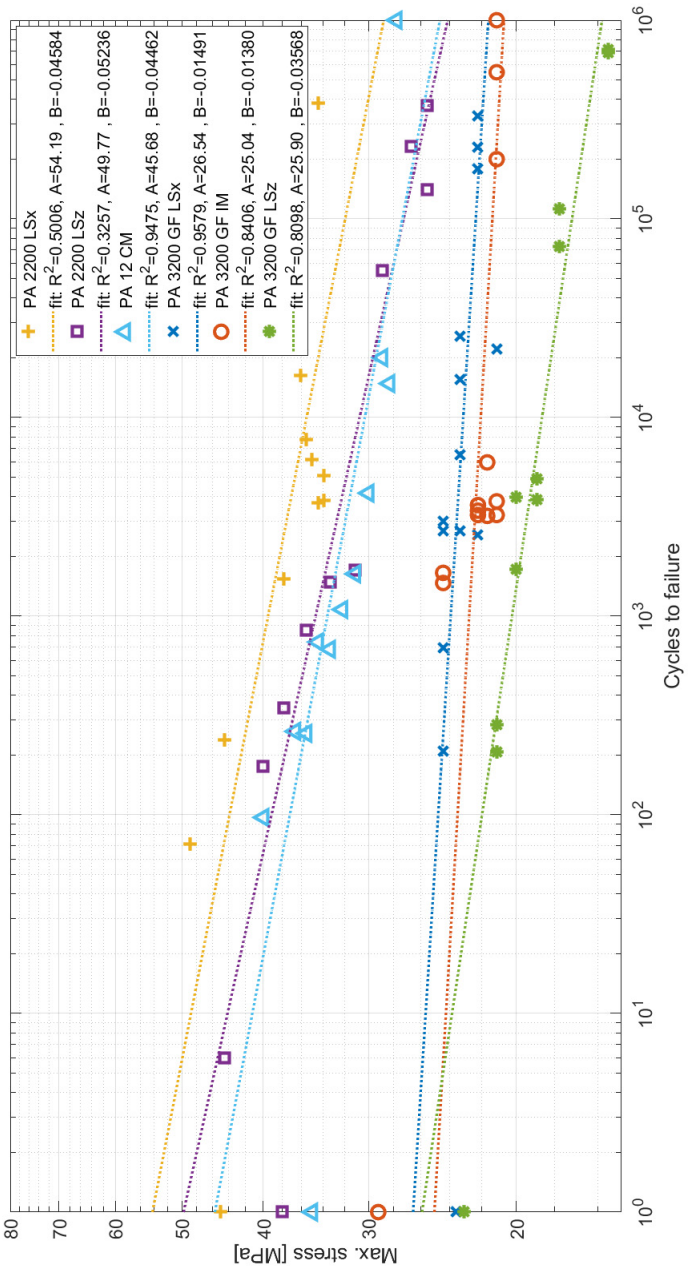

Figure 7: Fatigue data (SN curves) on a double logarithmic scale for the different materials glass bead filled PA12 and regular, unfilled PA12 (PA3200 and PA2200, PA12, respectively) and manufacturing processes (LSx, LSz, CM, IM), complemented with corresponding UTS values at 1 cycles. Except for the UTS values (datapoints at 100), all datapoints are included for the curve fitting. When plotted on a double logarithmic scale, the datapoints closely match a straight line following the Basquin law with equation 3

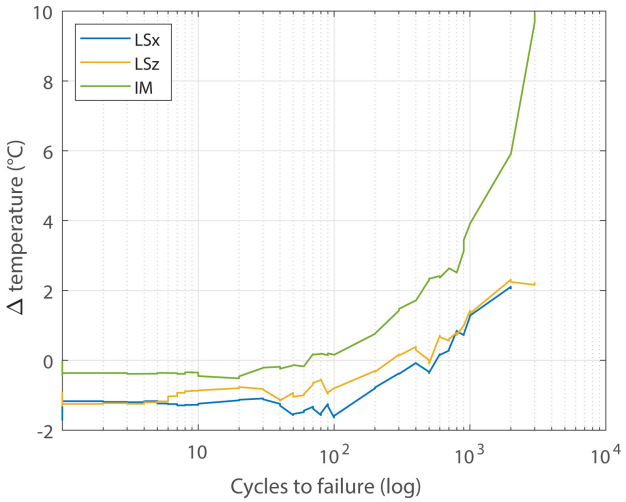

Figure 8: Temperature accumulation of glass bead filled PA12 samples produced by LS and IM during fatigue testing with a similar amount of 'cycles to failure'

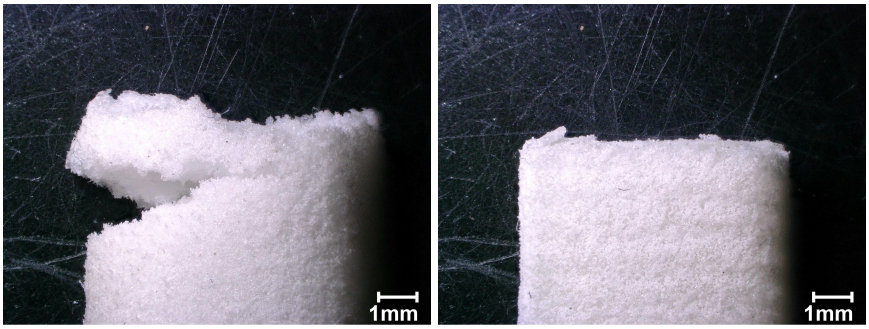

Figure 9: Fracture profiles of a glass bead filled PA12 samples produced by LS in the x-direction (left) and z-direction (right) after fatigue testing

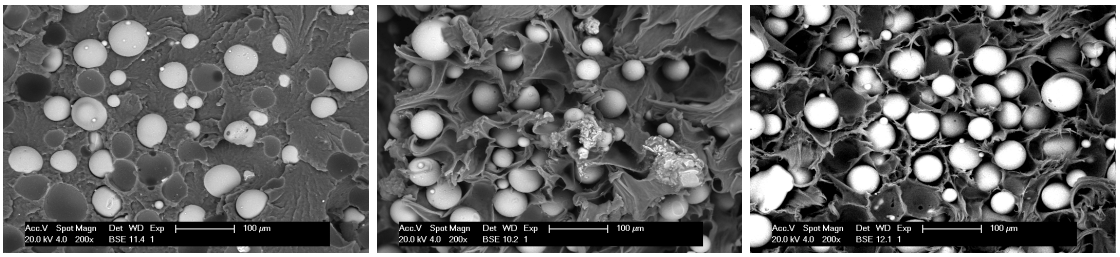

Figure 10: SEM observations of the fracture surfaces of glass bead filled PA12 samples produced by IM (left) and LS in the x-direction (middle) and z-direction (right) after fatigue testing

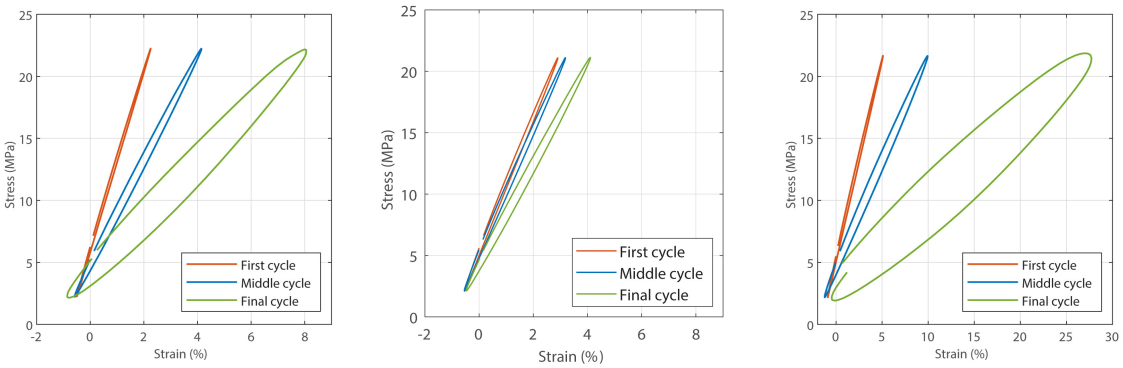

Figure 11: Hysteresis loops for glass bead filled PA12 samples produced by LS in the x-direction (left), z-direction (middle) and by IM (right) during the first, middle and final load cycle of fatigue testing with a mean stress of 12 MPa

To further analyse the thermo-mechanical behaviour of the glass bead filled PA12 samples subjected to fatigue testing, hysteresis loops (stress plotted as function of strain for separate load cycles) for the first, middle and final load cycles were plotted as shown in Figure 11. Although the glass bead filled PA12 samples in this study are subjected to tension-tension fatigue testing, the same phenomena happening during tension-compression fatigue testing are expected which were thoroughly investigated in previous research [3, 26]. For the IM samples, when the glass transition region is reached due to the self-heating effect discussed previously, the amorphous chains soften and lose their stiffness leading to larger deformations. This can be seen in Figure 11 as the decreased slope of the hysteresis loops in the final cycle before fatigue failure which was also noted in previous research on regular, unfilled PA12 [3].

Furthermore, the area within the hysteresis loops equals the energy loss during given load cycle [3]. During the first load cycles the energy loss is small for all the samples (LS and IM) resulting in a hysteresis loop resembling an almost straight line. Reaching the middle cycle of the fatigue life of the samples, a slight increase in the area within the hysteresis loops can be noted which means that there is a small loss of energy. As explained before, when the glass transition range is reached, the molecular mobility increases with an energy dissipation in the form of heat as a result. This dissipated energy and temperature increase is also indicated by the area within the final hysteresis loops, which is more pronounced for the IM samples than the LS samples as can be seen in Figure 8 and Figure 11. This is because the IM samples have a larger amount of amorphous chains as a result of the rapid cool downs associated with the IM process.

The energy losses due to heat dissipation were quantified by calculating the integrals and therefore the areas below the loading and unloading portions of the load-displacement hysteresis curves. By subtracting these values, the energy dissipated as heat E_d for each cycle is obtained. The loss factor η can then be calculated with Equation 4:

$$\eta = \frac{E_d}{2 \cdot \pi \cdot E_p} \tag{4}$$

Here, E_p is the maximum potential energy, which is equal to the area under the force-displacement curve corresponding to the loading phase of the hysteresis cycle. Calculated values for E_d of the final cycle and η can be seen in table 7.

When the hysteresis loops of the final cycle before fatigue failure of the glass bead filled PA12 samples produced by IM and LS are compared, the following observations can be made.

- The previous assumption of the intralayer fracture being less brittle than interlayer fracture is confirmed. The decrease in slope and corresponding higher energy dissipation and loss factor of the hysteresis loop of the final cycle before failure of the LSz sample is much less pronounced compared to the LSx and IM samples. This indicates poor adhesion between layers leading to damage accumulation, proving once again that LS samples are weaker in the z-direction than in the x-y-plane.

- The decrease in slope and energy losses of the final cycle before failure and the percentage of strain of the IM sample is much higher compared to both LS samples. It is expected that because of

Table 7: Energy dissipated by the regular and glass filled samples at the final cycle of fatigue testing with a mean stress of 20 MPa and 12 MPa for the regular and glass filled samples respectively

material		glass bead filled PA12 (PA3200 GF)		
parameter	unit	LSx	LSz	IM
E_d	[J]	96,49	22,26	544,70
η	[%]	3,32	1,46	4,96

material		regular PA12 (PA2200)		regular PA12
parameter	unit	LSx	LSz	CM
E_d	[J]	188,70	165,11	283,11
η	[%]	3,21	2,91	4,09

the applied temperature and pressure during IM, samples with a higher density are produced with good adhesion of the glass beads to the polyamide matrix. The IM polymer parts are more dense and more amorphous because of the rapid cool down after IM processing. This is different from LS, where the samples are kept at a certain preheating temperature and a relatively slow cooling cycle, which allows a higher degree of crystallinity in the samples. The amorphous chains will reach the glass transition region and lose stiffness due to thermal activity and energy dissipation in the form of heat. As discussed, there are more amorphous chains present in the IM samples than in the LS samples, therefore the stiffness of these IM samples will decrease more and the samples will experience larger deformations at the same stress levels which was clearly seen during fatigue testing.

These observations are confirmed by the results (Table 7) of the calculations of the energy losses and related loss factors (equation 4). It is immediately clear that both the energy loss and the loss factor are larger for the IM samples than for the LS samples. The LSz samples show slightly smaller energy losses than the LSx samples. This is in accordance with the reasoning given earlier; the IM samples have a larger amount of amorphous chains, which dissipate more heat when the glass transition region is reached due to an increase in molecular mobility. The slightly lower energy dissipation for the LSz samples can be attributed to the evolution of (more) damage mechanisms in these samples.

4.3 Comparison glass bead filled PA12 with regular, unfilled PA12

In this section the glass bead filled PA12 (PA3200 GF) and regular PA12 (PA2200/12) samples are taken into consideration. The focus is on the comparison of processed materials and its influence on quasi-static and fatigue performance.

4.3.1 Quasi-static performance

As mentioned in section 4.2, tensile tests were performed on samples of each category (production processes: LS, IM and CM and materials: glass bead filled PA12 (PA3200 GF), regular, unfilled PA12 (PA2200 and PA12)). The results of these tests are summarized in Table 6.

It is clear from Table 6 that the E-modulus of the glass bead filled samples is systematically higher compared to all regular, unfilled PA12 samples, as expected. This improvement of glass bead filled samples is most clearly visible for the injection moulded samples, compared to their compression moulded counterparts without glass beads. It is expected that because of the applied temperature and pressure during IM and CM, samples with a higher density are produced, leading to high values of strength and stiffness. Indeed, all glass bead filled samples are outperforming regular, unfilled samples in terms of stiffness because of the known higher stiffness of the present glass beads, and because of the good adhesion of the glass particles to the polyamide matrix.

As visible in Table 6, the stiffness is increased due to the addition of glass beads. However, the UTS shows a clear decrease, which is more than likely due to an imperfect glass/PA12 interface. The reason for this is expected to be related to debonding of the polymer matrix from the glass beads upon significant deformation of the samples. This phenomenon is not happening in the early stage of deformation where the bond between filler and matrix is considered strong, and where the E-modulus is determined as the slope of the initial stress-strain curve. It occurs later, upon further deformation, and hence significantly impacts the UTS and the strain at failure. Debonded glass beads cannot carry any load and will even

lead to stress concentrations in the remaining matrix, leading to lower strength and reduced strain at fracture.

For the CM samples, a slight increase in tensile stress can be noted at the end of the test for some samples (Figure 6). This is a consequence of strain hardening. This phenomenon occurs in the CM samples because they have more amorphous chains with the potential to strain harden when compared to LS samples [27]. It is expected that this strain hardening is limited for the glass bead filled IM samples due to the presence of the glass beads.

4.3.2 Fatigue performance

In-line with the earlier discussed phenomena of the quasi-static performance, the fatigue or SN-data in Figure 7 indicates two rather distinct regions: the upper region where the regular polyamide 12 (PA 2200 and PA12) datapoints are gathered, and a lower region where the glass bead filled polyamide 12 (PA 3200 GF) data can be seen.

It is evident from these datapoints that the regular, unfilled polyamide samples outperform the glass bead filled polyamide samples for all manufacturing methods, and for all applied maximum stress levels in fatigue, as well as for quasi-static loading (at cycle 1). The reason for this is most likely the fact that upon significant or repeated deformation, the glass beads detach from the polyamide matrix and cannot carry any load whilst introducing stress concentrations at the same time, leading to significantly reduced fatigue lives for all applied stress levels. Scanning electron microscopy observations of the fracture surfaces of the tested LS samples show this detachment of the glass beads from the matrix material and can be seen in Figure 10. Scanning electron microscopy observation of the fracture surface of the tested IM samples, also seen in Figure 10, shows much less micro-ductile areas and debonding of the glass beads from the matrix material. In this case crack initiation as result of the present glass beads took place before the filler-matrix interface failed which was also noticed in previous research [28].

The difference between glass bead filled and regular, unfilled samples seems to reduce in the high cycle fatigue regime, where lower loads are applied and where the bond between filler and matrix can remain largely intact. This appears not to be the case for the glass bead filled PA12 LSz samples, which show the lowest fatigue strength out of all samples tested. The reason for this is believed to be the fact that for any laser sintered part, the intralayer bonding and strength (within one layer) is higher than the inter-layer bonding and strength (between layers) [18]. This is mostly due to the relative large interlayer time, leading to imperfect bonding of successive layers which was also discussed in section 4.2.

In the frame of the current study, the weaker properties of the vertically built (z-direction) LS samples are assumed to couple with the weakening of glass bead debonding, leading to the lowest fatigue resistance of glass bead filled PA12 LSz samples as shown in Figure 7.

4.3.3 Hysteresis

Similar conclusions can be drawn when comparing the thermo-mechanical behaviour during fatigue testing of the glass bead filled PA12 samples with the regular, unfilled PA12 samples. Also for the regular, unfilled PA12 hysteresis loops for the first, middle and final load cycles were plotted and can be seen in Figure 12. Again, these samples were subjected to tension-tension fatigue testing though the same phenomena happening during tension-compression fatigue testing are expected which were thoroughly investigated in previous research [3, 26].

As mentioned in section 4.2, mostly for the IM and CM samples, amorphous polymer chains will soften once the semi-crystalline PA12 material reaches the glass transition region due to self-heating, resulting in reorientation of these chains. After this reorientation of the polymer chains, crystallisation might take place when the tension-tension loading is stopped. However, the tension-tension loading is applied until failure, resulting in a decrease off the stiffness and leading to larger deformations of the tested PA12 samples at same stress levels. At the glass transition region, the amorphous chains will soften more and can lose their stiffness due to the thermal activity and dissipative effect. This can be noticed in Figure 12 as the decreased slope of the hysteresis loops in the final cycle before fatigue failure, which was also discussed in previous research by Van Hooreweder et al. [3].

As mentioned in section 4.2, the area within the hysteresis loops equals the energy loss during given load cycle [3]. Also for the unfilled PA12 samples (LS and CM), during the first load cycles the energy loss is small resulting in a hysteresis loop resembling an almost straight line. Reaching the middle cycle of the fatigue life of the samples, a slight increase in the area within the hysteresis loops can be noted which means that there is a small loss of energy. As explained before, when the glass transition range is reached, the molecular mobility increases with an energy dissipation in the form of heat as a result. For

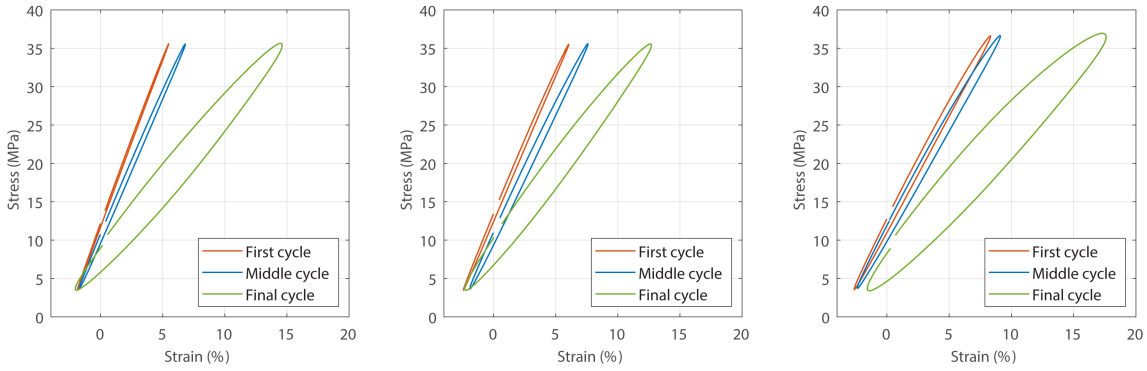

Figure 12: Hysteresis loops for regular, unfilled PA12 samples produced by LS in the x-direction (left), z-direction (middle) and by CM (right) during the first, middle and final load cycle of fatigue testing with a mean stress of 20 MPa

the unfilled PA12 samples the temperature of the samples was not registered, though, the area within the final hysteresis loops increases significantly as can be seen in Figure 12. From this, an increase in dissipated energy in the form of a temperature increase in the samples can be assumed which is more pronounced for the CM samples compared to the LS samples.

Also for the unfilled PA12 samples, the energy losses due to heat dissipation were quantified and the energy dissipated as heat E_d is obtained for each cycle. And also the loss factor η was calculated with equation 4. Calculated values for E_d of the final cycle and η can be seen in Table 7.

When the hysteresis loops of the final cycle before fatigue failure of the regular, unfilled PA12 samples produced by LS and CM are compared, the following observations can be made which are similar to those made in section 4.2.

- Again, the assumption of the intralayer fracture being less brittle than interlayer fracture is confirmed. The decrease in slope and corresponding higher energy dissipation and loss factor of the hysteresis loop of the final cycle before failure of the LSz sample is much less pronounced compared to the LSx and CM samples. For the LSz samples also some softening of the polymer chains will happen once the glass transition region is reached. However, here the observed performance loss followed by fatigue failure is dominated by damage accumulation due to poor adhesion between layers in the z-direction (interlayer) and the related porosity content. This is also confirmed when the fracture profiles after fatigue testing are investigated by optical microscopy. In Figure 13 fracture profiles after fatigue testing of regular, unfilled PA12 samples produced by LS in the x-direction and CM are shown which shows signs of yielding in the samples that lead to ductile fatigue failure. The fracture profile after fatigue testing of regular, unfilled PA12 samples produced by LS in the z-direction looks almost identical to the fracture profile of the glass bead filled PA12 LSz samples which is displayed in Figure 9 (right) which shows absolutely no signs of yielding and a pronounced brittle fracture. This brittle fracture is confirmed by comparing scanning electron images of the fracture surfaces of regular, unfilled PA12 samples produced by LS in the x-direction and z-direction after fatigue testing shown in Figure 14.

- The decrease in slope of the final cycle and energy losses before failure and the percentage of strain of the CM sample is much higher compared to both LS samples. It is expected that because of the applied temperature and pressure during CM, samples with a higher density are produced. The CM polymer parts are also more amorphous because of the relatively faster cooling rates associated with the process. This results in more amorphous polymer chains that will soften once the glass transition region is reached, leading to a larger decrease in stiffness when compared to LS samples. The samples will experience larger deformations at the same stress levels which was clearly seen during fatigue testing. Finally, the samples will fail due to the thermal activity and dissipative effect. This is different from LS, where the samples are kept at a certain preheating temperature and a relatively slow cooling cycle, which allows a higher degree of crystallinity in the samples, resulting in less amorphous polymer chains to soften and reorient.

The same conclusions as drawn for the glass bead filled samples, can be drawn from the unfilled PA12 sample results, where the CM samples show much higher energy losses and loss factors when compared

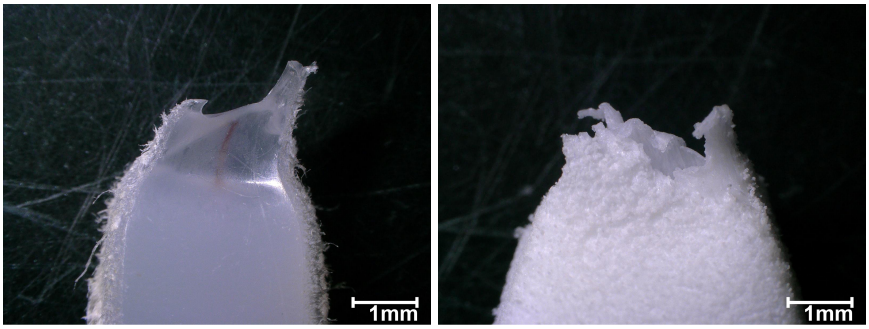

Figure 13: Fracture profiles of regular, unfilled PA12 samples produced by LS in the x-direction (left) and CM (right) after fatigue testing

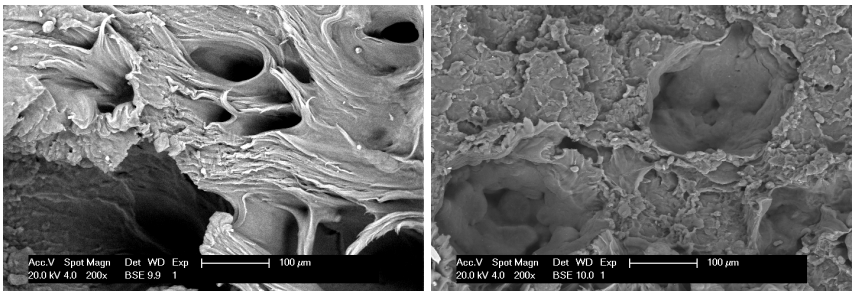

Figure 14: SEM observations of the fracture surfaces of regular, unfilled PA12 samples produced by LS in the x-direction (left) and z-direction (right) after fatigue testing

to LSx and LSz samples, and again the LSz samples show slightly lower energy losses than their LSx counterparts.

4.4 Comparison with literature on glass bead filled polymers

The results presented in this work are in line with previously published works dealing with altering the mechanical performance of polyamide or similar polymers by addition of glass beads or glass fibres. Mostly quasi-static mechanical testing was conducted from which following conclusions were made [29–31]:

- Glass beads can significantly increase the stiffness and toughness of the polymer material, though, an upper limit in filler concentration can be reached after which all mechanical properties decrease.
- Glass beads significantly decrease the tensile strength and ductility, strain at fracture with increasing glass bead content.
- The results are highly dependent on the interfacial adhesion, the bond between the matrix material (polymer) and the glass beads.

A. Bernasconi and C. Armanni studied the role of fillers in the fatigue behaviour of short glass fibre reinforced polyamide and concluded that glass beads reduced the fatigue lives of the samples. And as earlier mentioned, the glass beads successfully contribute to the increased stiffness of the material but act as stress raisers and thus accelerate crack formation in fatigue testing [28]. Which can also be concluded in this work.

5 Conclusions

The quasi static and fatigue performance of as-built glass bead filled polyamide parts produced by laser sintering (LS) and injection moulding (IM) compared to as-built regular, unfilled polyamide parts produced by laser sintering and compression moulding (CM) was investigated in this study. To understand and investigate the occurring failure mechanisms, scanning electron observations, thermal properties

and hysteresis behaviour was taken into account and analysed. The most important conclusions of this research are summarised below.

- Cyclic mechanical loading in combination with temperature effects controls the fatigue failure of all the specimens [3].
- Addition of glass beads to polyamide successfully increases stiffness of the samples for both production techniques (LS and IM) but clearly goes at the expense of UTS and strain at fracture. In addition, a significant negative influence is noted on the fatigue performance of all glass bead filled polyamide samples. The reason for this is most likely the fact that upon significant or repeated deformation, the glass beads detach from the polyamide matrix, cannot carry any load whilst at the same time introducing stress concentrations, leading to significantly reduced fatigue lives for all applied stress levels.
- The glass bead filled polyamide samples produced by laser sintering in the z-direction show the lowest fatigue strength of all samples tested which is believed to be caused by the fact that the intralayer bonding and strength (within one layer) is higher than the interlayer bonding and strength (between layers). This is mostly due to the relative large interlayer time, leading to imperfect bonding of successive layers. This weak inter-layer binding is assumed to couple with the weakening of glass bead debonding, leading to the lowest fatigue resistance of glass bead filled PA12 LSz samples.

Thus, future work is needed to successfully develop a way of introducing reinforcements in the laser sintering process to optimise mechanical properties, such as strength and stiffness of produced parts, without degrading the fatigue performance. This could be achieved by adding fibre reinforcements with a significant length (same as or longer than the critical length required for complete stress transfer from the matrix to the fibre up to its ultimate tensile strength [16, 32]) to the samples produced by laser sintering. However, for this fibre addition a new system should be developed to overcome problems with powder flowability and impregnation of the fibres. In addition, the vertical build direction (z-direction) during the laser sintering process is known as the weakest direction to build functional parts, which is also highlighted in this research. By adding macroscale fibre reinforcements opportunities might arise to also tackle this weakest, limiting factor of the laser sintering process, which can lead to broader application of LS components in industry.

6 Acknowledgements

This work was supported by a bilateral collaboration with Ford Research and Advanced Engineering Europe, by the European Space Agency (ESA) as part of a co-funded PhD OSIP project AO8_3-17001_SC_30750, and the research fund of KU Leuven through C3-project C3/20/083. The authors would like to thank Robin Koekoekx for his assistance with the Collins extruder and pelletizer, Yves Santermans for his assistance with the injection moulding process and Jeroen Soete for the CT scanning of the powder.

References

[1] J. P. Kruth, X. Wang, T. Laoui, and L. Froyen, "Lasers and materials in selective laser sintering," *Assembly Automation*, vol. 23, no. 4, pp. 357–371, 2003.

[2] P. Parandoush and D. Lin, "A review on additive manufacturing of polymer-fiber composites," *Composite Structures*, vol. 182, pp. 36–53, 2017.

[3] B. Van Hooreweder, D. Moens, R. Boonen, J. P. Kruth, and P. Sas, "On the difference in material structure and fatigue properties of nylon specimens produced by injection molding and selective laser sintering," *Polymer Testing*, vol. 32, pp. 972–981, aug 2013.

[4] J. Frketic, T. Dickens, and S. Ramakrishnan, "Automated manufacturing and processing of fiber-reinforced polymer (FRP) composites: An additive review of contemporary and modern techniques for advanced materials manufacturing," *Additive Manufacturing*, vol. 14, no. 4, pp. 69–86, 2017.

[5] J. Kruth, G. Levy, R. Schindel, T. Craeghs, and E. Yasa, "Consolidation of Polymer Powders by Selective Laser Sintering," in *International Conference on Polymers and Moulds Innovations*, pp. 15–30, 2008.

[6] J. P. Kruth, P. Mercelis, J. Van Vaerenbergh, L. Froyen, and M. Rombouts, "Advances in selective laser sintering," in *Advanced Research in Virtual and Rapid Prototyping*, pp. 59–70, 2003.

[7] T. J. Gill and K. K. B. Hon, "Experimental investigation into the selective laser sintering of silicon carbide polyamide composites," in *Proceedings of the Institution of Mechanical Engineers, Part B: Journal of Engineering Manufacture*, vol. 218, pp. 1249–1256, 2004.

[8] W. Jing, C. Hui, W. Qiong, L. Hongbo, and L. Zhanjun, "Surface modification of carbon fibers and the selective laser sintering of modified carbon fiber/nylon 12 composite powder," *Materials and Design*, vol. 116, pp. 253–260, 2017.

[9] J. Kim and T. S. Creasy, "Selective laser sintering characteristics of nylon 6/clay-reinforced nanocomposite," *Polymer Testing*, vol. 23, no. 6, pp. 629–636, 2004.

[10] J. Bai, R. D. Goodridge, R. J. Hague, and M. Song, "Improving the Mechanical Properties of Laser-Sintered Polyamide 12 Through Incorporation of Carbon Nanotubes," *Polymer engineering and science*, 2013.

[11] L. Cheung and I. Gibson, "Effects of graphite powder on the laser sintering behaviour of polycarbonate," vol. 8, no. 4, pp. 233–242.

[12] T. Kozior, "Assessment of mechanical properties of pa 3200 gf polyamide models made by SLS," *Czasopismo Techniczne*, vol. 11, no. 115, pp. 181–186, 2018.

[13] H. Chung and S. Das, "Processing and properties of glass bead particulate-filled functionally graded Nylon-11 composites produced by selective laser sintering," *Materials Science and Engineering A*, vol. 437, no. 2, pp. 226–234, 2006.

[14] A. Mousah, *Effects of filler content and coupling agents on the mechanical properties and geometrical accuracy of selective laser sintered parts in glass bead-filled polyamide 12 composites.* PhD thesis, 2011.

[15] G. D. Goh, Y. L. Yap, S. Agarwala, and W. Y. Yeong, "Recent Progress in Additive Manufacturing of Fiber Reinforced Polymer Composite," *Advanced Materials Technologies*, vol. 4, no. 1, pp. 1–22, 2019.

[16] P. Forderhase, K. Mc Alea, and R. Booth, "The development of an SLS composite material," in *International solid freeform fabrication proceedings*, pp. 287–297, 1995.

[17] A. J. Cano, A. Salazar, and J. Rodríguez, "Effect of temperature on the fracture behavior of polyamide 12 and glass-filled polyamide 12 processed by selective laser sintering," *Engineering Fracture Mechanics*, vol. 203, no. July, pp. 66–80, 2018.

[18] A. Salazar, A. J. Cano Aragón, and J. Rodríguez, "Fatigue life assessment of polyamide 12 processed by selective laser sintering. Damage modelling according to fracture mechanics," *Rapid Prototyping Journal*, vol. ahead-of-p, no. ahead-of-print, 2021.

[19] R. D. Goodridge, C. J. Tuck, and R. J. Hague, "Laser sintering of polyamides and other polymers," *Progress in Materials Science*, vol. 57, no. 2, pp. 229–267, 2012.

[20] B. Van Hooreweder, *Development of Accelerated Multi-axial Fatigue Tests Based on Scaling Laws (Ontwikkeling van versnelde multi-axiale levensduurtesten op basis van schaalwetten)*. PhD thesis, 2013.

[21] S. Terekhina, T. Tarasova, S. Egorov, L. Guillaumat, and M. L. Hattali, "On the difference in material structure and fatigue properties of polyamide specimens produced by fused filament fabrication and selective laser sintering," *International Journal of Advanced Manufacturing Technology*, vol. 111, no. 1-2, pp. 93–107, 2020.

[22] L. S. O. Pires, M. H. F. V. Fernandes, and J. M. M. de Oliveira, "Crystallization kinetics of PCL and PCL–glass composites for additive manufacturing," *Journal of Thermal Analysis and Calorimetry*, vol. 134, no. 3, pp. 2115–2125, 2018.

[23] S. Gogolewski, K. Czerntawska, and M. Gastorek, "Effect of annealing on thermal properties and crystalline structure of polyamides. Nylon 12 (polylaurolactam)," *Colloid and Polymer Science 1980 258:10*, vol. 258, pp. 1130–1136, oct 1980.

[24] T. Stichel, T. Frick, T. Laumer, F. Tenner, T. Hausotte, M. Merklein, and M. Schmidt, "A Round Robin study for Selective Laser Sintering of polyamide 12: Microstructural origin of the mechanical properties," *Optics and Laser Technology*, vol. 89, no. July 2016, pp. 31–40, 2017.

[25] L. Safai, J. S. Cuellar, G. Smit, and A. A. Zadpoor, "A review of the fatigue behavior of 3D printed polymers," *Additive Manufacturing*, vol. 28, no. April, pp. 87–97, 2019.

[26] B. Van Hooreweder, F. De Coninck, D. Moens, R. Boonen, and P. Sas, "Microstructural characterization of SLS-PA12 specimens under dynamic tension/compression excitation," *Polymer Testing*, vol. 29, no. 3, pp. 319–326, 2010.

[27] C. Miehe, S. Göktepe, and J. Méndez Diez, "Finite viscoplasticity of amorphous glassy polymers in the logarithmic strain space," *International Journal of Solids and Structures*, vol. 46, no. 1, pp. 181–202, 2009.

[28] A. Bernasconi and C. Armanni, "Role of Fillers in the Fatigue Behaviour of a Short Glass Fibre Reinforced Polyamide," in *Materials Science, Engineering*, 2008.

[29] L. Huang, Q. Yuan, W. Jiang, L. An, S. Jiang, and R. K. Li, "Mechanical and thermal properties of glass bead-filled nylon-6," *Journal of Applied Polymer Science*, vol. 94, no. 5, pp. 1885–1890, 2004.

[30] J. Z. Liang and R. K. Li, "Mechanical properties and morphology of glass bead-filled polypropylene composites," *Polymer Composites*, vol. 19, no. 6, pp. 698–703, 1998.

[31] E. Kuram, "Synergistic effect of glass bead and glass fiber on the crystalline structure, thermal stability, and mechanical, rheological, and morphological properties of polyamide 6 composites," *Journal of Composite Materials*, vol. 56, no. 3, pp. 441–453, 2022.

[32] R. G. Kleijnen, J. P. Sesseg, M. Schmid, and K. Wegener, "Insights into the development of a short-fiber reinforced polypropylene for laser sintering," *AIP Conference Proceedings*, vol. 1914, no. December, 2017.